Journal of Industrial Intelligence
https://www.acadlore.com/journals/JII

# Numerical Analysis of Viscosity and Surface Tension on Microdroplet Dynamics in Microelectromechanical Systems Applications

Somaiyeh Alizadeh[1], Razieh Abbasgholi Rezaei[2*]

[1] Department of Mechanical Engineering, RMIT University, VIC 3000 Melbourne, Australia
[2] Department of Mechanical Engineering, Urmia University, 5756151818 Urmia, Iran

* Correspondence: Razieh Abbasgholi Rezaei (r_rezaei_mec@yahoo.com)

**Received:** 07-23-2023 **Revised:** 09-13-2023 **Accepted:** 09-16-2023

**Citation:** S. Alizadeh and R. A. Rezaei, "Numerical analysis of viscosity and surface tension on microdroplet dynamics in microelectromechanical systems applications," *J. Ind Intell.*, vol. 1, no. 3, pp. 158–164, 2023. https://doi.org/10.56578/jii010303.



**Abstract:** Microelectromechanical systems (MEMS) have instigated transformative advancements, notably in controlled microdroplet generation, offering applications across diverse industrial sectors. Precise control of fluid quantities at microscales has emerged as pivotal for myriad fields, from microfluidics to biomedical engineering. In this investigation, the impacts of fluid viscosity and surface tension on microdroplet formation were meticulously studied. For this purpose, a microdispenser, actuated piezoelectrically and fitted with an 18-micrometer diameter nozzle, was employed. This setup facilitated precise fluid manipulation, enabling a systematic study of fluid behavior during droplet creation. Three fluids, specifically water, ink, and ethanol, were examined to decipher the influences of their inherent properties on microdroplet generation. Emphasis was laid on both primary and satellite droplets due to their direct implications in industrial applications. Observations revealed that fluids with elevated surface tension and diminished viscosity yielded larger microdroplets. Conversely, fluids manifesting greater surface tension underwent rapid breakup upon ejection, culminating in the genesis of several diminutive droplets. Such findings underscore the intricate relationship between fluid properties and droplet formation dynamics. This newly acquired understanding holds the potential to guide MEMS device design, ensuring the desired droplet size and distribution. Furthermore, these insights are poised to facilitate optimal microdispenser design and judicious fluid selection for applications spanning inkjet printing, microreactors, and drug delivery mechanisms.

**Keywords:** Microelectromechanical systems (MEMS); Microdispenser; Microdroplet; Surface tension; Viscosity

## 1 Introduction

Microdroplet production has been identified as integral to microscopic investigations spanning numerous scientific domains, encompassing biology, chemistry, medicine, and industrial applications. The controlled generation of microdroplets, owing to its multifaceted applications in 2D printers, 3D inkjet printing, biomedicine, fuel spraying, and other sectors such as chemical industries, pharmaceuticals, electronics, and micro-optical devices, has garnered pronounced attention [1, 2].

Two principal methodologies govern droplet generator operations: constant stream and drop-on-demand (DOD), contingent upon continuous and periodic flow rate demands. In the former, fluid is dispensed at a uniform rate, leading to a persistent liquid jet which disintegrates into minute droplets soon after expulsion from the nozzle. This phenomenon leverages the intrinsic instability of slender jets, termed the Rayleigh instability, facilitating an unceasing droplet stream. In contrast, DOD droplet gefnerators fashion droplets in response to external triggers, classifying them as non-pressure droplet generators [3].

Historically, Lord Rayleigh elucidated a mechanism by which a liquid column fractured into droplets [4]. This foundational insight catalyzed the inception of the inaugural practical inkjet apparatus, as documented by Siemens Elema in Sweden [5]. Subsequent investigations, spearheaded by Li et al. [6], examined pulsed microjet flows ejected from a piezoelectric inkjet printer. Analyses of diverse operating voltages and ejection frequencies discerned that augmented voltages induced the emergence of satellite droplets and elongated maximum ligament lengths. Several parameters, encompassing ink attributes, ejection modalities, and nozzle configurations, were recognized to mold the characteristics of primary and satellite droplets [7, 8].

A prevailing aspiration in microdroplet creation has been the minimization of droplet dimensions, necessitating the production of droplets with diameters smaller than that of the nozzle [9]. One approach to realize this entails the utilization of constricted nozzles; however, diminutive nozzles exhibit heightened susceptibility to obstructions [10, 11]. Moreover, while a slimmer nozzle escalates surface tension and viscous forces, necessitating augmented propulsive pressure, it concurrently curtails flow resistance, thus moderating the required driving pressure [10, 11].

Significantly, fluid characteristics, especially surface tension and viscosity, exert profound influences on droplet formation. Droplet dimensions were found to amplify nearly linearly with the nozzle diameter, and analogous linear relationships were observed between droplet volume, pulse voltage, and pulse width [12, 13]. Curiously, loudspeakers have been proposed as noise generation sources in DOD generators [14, 15]. Alternative droplet generators operate by administering a gaseous or liquid pressure pulse to eject the liquid, designating them as pneumatic drop generators [16, 17]. In the realm of microfluidics, T-shaped connections and FFD (flow-focusing device) flow concentrators have predominantly been employed for droplet partitioning, although dielectrophoresis and electrowetting on dielectric are emerging techniques [18]. Furthermore, Crowley's theoretical exploration into electrohydrodynamic drop production (EHD) merits acknowledgment [19, 20].

This investigation delves into the ramifications of disparate fluid viscosities and surface tensions on primary and satellite droplet formations, alongside droplet formation velocities. Employed for numerical assessments and simulations is the FLUENT 6.3 software, paired with the Volume of Fluid (VOF) methodology. It is anticipated that these findings will catalyze advancements in MEMS technology, ushering in refined microdroplet manipulation techniques by facilitating judicious fluid selection for uniform droplet sizes and the curtailment of satellite droplet emergence.

Subsequent sections employ the VOF with explicit parameters within the FLUENT software, aiming to discern the influences of fluid attributes and excitation magnitudes on primary and satellite droplet dimensions.

## 2 Numerical Analysis

The dynamics of two-phase, incompressible flows comprising liquid droplets and gas have been analyzed. Within this scope, the VOF method, an Eulerian approach, was employed. In this method, the computational domain was divided into a grid, and the volume fraction of each fluid within every grid cell was tracked. The interface between liquid droplets and gas was effectively captured by determining the volume occupied by each fluid at any given instance. This allowed for detailed modeling of intricate interactions between the phases, encompassing behaviors such as breakup and coalescence. A salient advantage of the VOF method lies in its adaptability to handle moving interfaces, coupled with its capacity to address substantial density and viscosity disparities between the fluids. Depending on the specific problem under analysis, the employment of a fixed or moving mesh in the VOF method was considered. In scenarios where significant deformations or complex motions were observed at the interface between the liquid and gas phases, a moving mesh approach was favored to track the evolving interface meticulously. Conversely, a fixed mesh was deemed apt for relatively simple flow scenarios or when computational efficiency was prioritized.

Central to the VOF method is a numerical characteristic function, denoted as $\alpha$, which assumes values between zero and one, facilitating the identification of the interface between two immiscible fluids. Specifically, $\alpha$ is representative of the volume fraction occupied by one of the fluids within a given volume, $V$. It was defined as:

$$\alpha^k = \lim_{V\to\infty} \frac{1}{V} \iiint \chi^k(x,y,z,t)dV \tag{1}$$

Here, an $\alpha$ value of 0 signifies the presence of one fluid, whereas $\alpha$ = 1 denotes the presence of the other fluid. When implemented within a computational mesh, a volume fraction value between zero and one was identified, signifying a shared interface between the fluids and offering a portrayal of their respective occupied portions within a specific cell volume.

Significantly, the VOF method was employed to evolve the volume fraction while upholding the mass continuity law. Calculations for the mixture's density, as well as the viscosity and thermal conductivity of the two-phase flow, were based on the following equations for multi-phase flows:

$$\rho^m = \sum_{k=1}^{N_p} \alpha_\mathrm{k}\rho_\mathrm{k} \tag{2}$$

$$\lambda^m = \sum_{k=1}^{N_p} \alpha_\mathrm{k}\lambda_\mathrm{k} \tag{3}$$

$$\mu^m = \sum_{k=1}^{N_p} \alpha_k \mu_k \tag{4}$$

In these equations, $N_p$ denotes the number of phases involved in the analysis.

In the endeavor to explore the dynamics of two-phase, incompressible flows, the Coupled Pressure-Velocity formulation was employed within the FLUENT software. An implicit method was selected for linearization purposes. The VOF method, with explicit parameters, served as the computational foundation for two-phase flow calculations. Notably, $N_p$ was fixed at 2, and a Courant number of 0.25 was chosen. Such parameters have been identified to yield precise insights into the interplay between liquid droplets and gas within the system.

The governing continuity equation for the flow under study is articulated as:

$$\partial\rho/\partial t + \nabla \cdot (\rho u) = 0 \tag{5}$$

In this formulation, $\partial\rho/\partial t$ epitomizes the density's rate of change, with $\nabla$ representing the gradient operator. The symbols $\rho$ and $u$ respectively signify the fluid's density and flow velocity. For the special case of incompressible flow, the continuity equation is reduced to:

$$\nabla \cdot u = 0 \tag{6}$$

Flow dynamics within the studied system are captured by the seminal Navier-Stokes equations. With the assumption of an incompressible flow, coupled with constant dynamic viscosity and fluid density, the Navier-Stokes equation is reformulated as:

$$\rho(\partial u/\partial t + u \cdot \nabla u) = -\nabla P + \mu\nabla^2 u + \rho g \tag{7}$$

In the aforementioned equation, $P$, $\mu$, and g designate pressure, dynamic viscosity, and gravitational acceleration, respectively. It should be highlighted that due to the diminutive fluid dimensions inherent to this study, the effects of the gravitational field were disregarded and hence were excluded from the momentum equation.

Of particular interest to this investigation is the DOD type inkjet, driven by piezoelectric stimulation, as illustrated in Figure 1. Within piezoelectric droplet generators, a transformation occurs where piezoelectric materials, under the influence of an electric potential difference, undergo a physical displacement. This displacement is either directly or indirectly responsible for droplet formation.

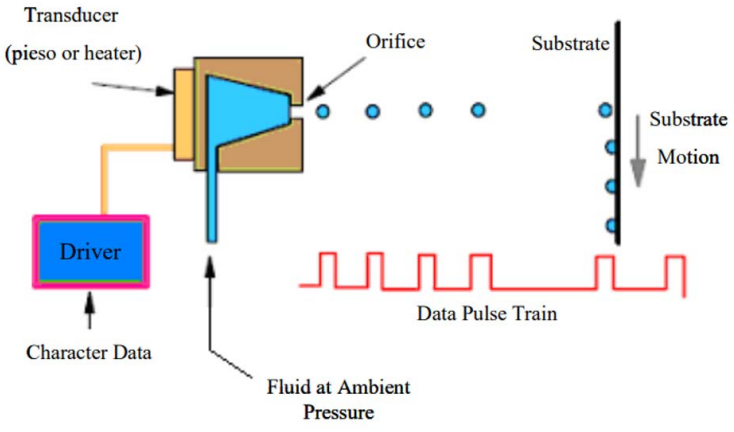


**Figure 1.** Mechanism of a DOD-type dropper

This section elucidates the fluidic properties and geometric considerations, with particular emphasis on discerning the common phase between liquid and gas in a piezoelectrically actuated inkjet printer within a constricted time span. Figure 2 provides a schematic visualization of the nozzle. Due to the axial symmetry of the nozzle, it has been deemed amenable for two-dimensional simulation. The domain under investigation bifurcates into two salient regions: the liquid chamber and the air chamber. The geometric dimensions are delineated in Table 1. To facilitate efficacious computational procedures, a uniform Quadrilateral mesh, encompassing 2400 cells, was adopted.

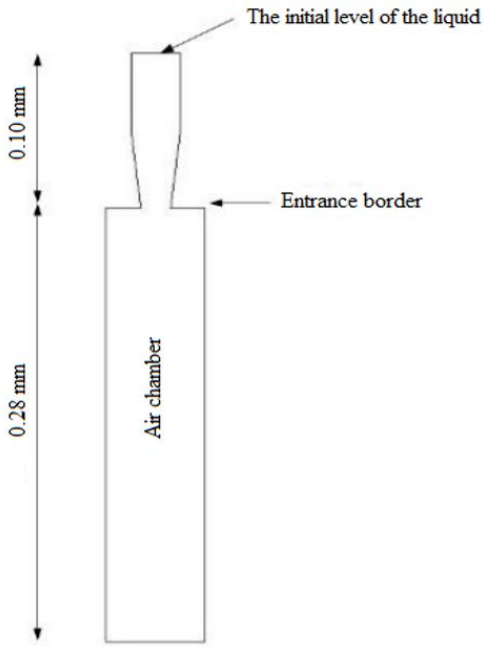


**Figure 2.** Schematic representation of the nozzle's geometry

**Table 1.** Geometrical delineations of the ink and air chambers

| **Dimensions of Ink and Air Chamber** | |
|---|---|
| Radius of the ink cylinder housing | 0.015 mm |
| Length of ink cylinder chamber | 0.050 mm |
| The final radius of the conical ink chamber | 0.009 mm |
| The length of the ink cone chamber | 0.050 mm |
| Air chamber radius | 0.030 mm |

In the initial phase, water was found to inundate the nozzle, with the auxiliary chamber occupied by air. Upon the release of water from the inlet boundary, a surge in its velocity from nil to 3.58 m/s was observed, which subsequently attenuated following a cosine function. Post a lapse of 10 microseconds, this velocity reverted to its initial state. The computational endeavors spanned a duration of 30 microseconds and were executed incrementally. Owing to the diminutive dimensions integral to the study, gravitational forces were omitted from the analysis. To encapsulate an accurate portrayal of the fluid dynamics, both surface tension and wetting angle factors were integrated. The pertinent values associated with the viscosity, density, and surface tension of the introduced fluid have been cataloged in Table 2.

**Table 2.** Salient physical attributes of the fluids under study

| **Properties of Studied Fluids** | | | |
|---|---|---|---|
| Fluid | $\mu(\mathrm{kg/m.s})$ | $\rho\,(\mathrm{kg/m^{3)}}$ | $\sigma(\mathrm{dyn/cm})$ |
| Ink | 0.0037 | 1070 | 32 |
| Water | 0.001003 | 998.2 | 73.5 |
| Ethanol | 0.0012 | 790 | 22.39 |

To furnish a comparative assessment of varied substances' implications on the droplet's velocity and morphology, and to elucidate the genesis of secondary droplets, substances like ink, water, and ethanol were employed. Simulations were meticulously tailored to incorporate the unique properties of each fluid.

## 3 Results

In the exploration of droplet formation through the DOD process, velocity profiles and phase contours associated with fluids of varied viscosities and surface tensions were scrutinized. Simulation outcomes unveiled a necking phenomenon at the droplet's tail during fluid column ejection. It was observed that, upon reaching the nozzle exit, the initial necking precipitated droplet detachment. Subsequently, as the fluid thread diminished further, a

second necking manifested near the droplet's head, leading to the distinct onion-like droplet morphology depicted in Figure 3.

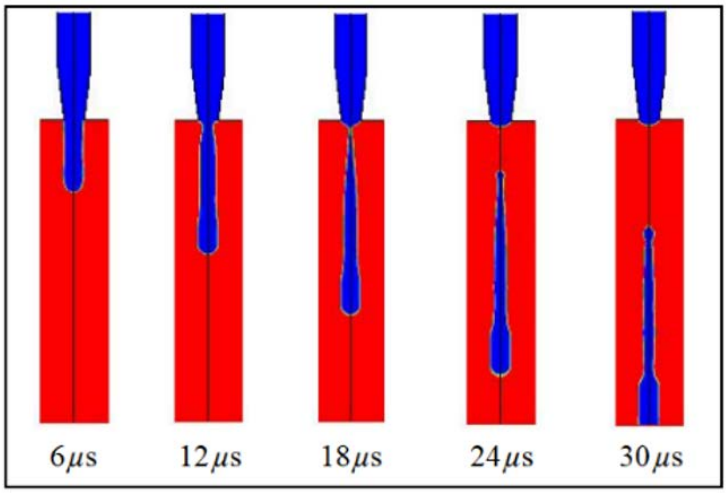


**Figure 3.** Ink contours during diverse temporal intervals: 6, 12, 18, 24, and 30 $\mu$s

In specific instances, detachment of the droplet tail was identified, culminating in the emergence of satellite droplets. Such occurrences are deemed inauspicious in DOD methodologies, as they compromise the precision of the printing technique. Notably, fragmentation of the primary droplet thread into several primary droplets was evident, especially with water, attributed to its expedited necking mechanism. The genesis of multiple principal droplets is also regarded as detrimental within DOD droplet production paradigms.

Focused analyses on the dynamics of two-phase, incompressible flows-comprising liquid droplets and gas-accentuated the droplet ejection, necking, and disintegration stages. Figure 4 delineates these phases, unveiling unique fluid behaviors. In the nascent stages of droplet ejection, a conical form was predominantly observed in the droplet head region for the majority of fluids, with water being an exception, manifesting a more streamlined profile. This shape variation was attributed to the velocity profile at the nozzle exit. It was discerned that, at this juncture, surface tension exerted negligible influence on droplet morphology, maintaining consistent velocity and length across ejected droplets.

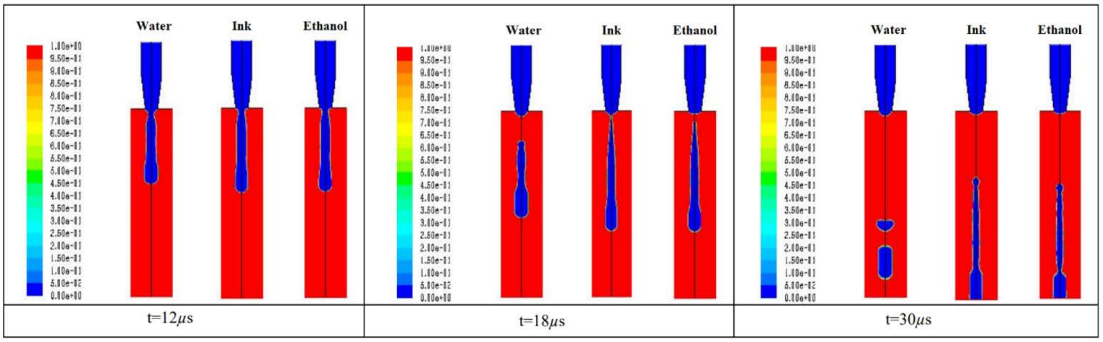


**Figure 4.** Injection and fluid elongation phases across diverse temporal intervals

In the necking phase, fluids with heightened surface tension exhibited escalated necking velocities and conspicuous droplet neck formations. For water, though the droplet neck was discernibly more expansive compared to high-viscosity fluids, it presented a less accentuated curvature at the droplet tip. This curvature disparity became more pronounced in other fluids. With diminishing fluid viscosity, the requisite length for droplet origination extended. Though fluids approximating ink viscosity exhibited continuous flows, water, possessing a notably superior surface tension, showcased a contracted droplet column span. Due to its smoother droplet head and augmented detachment velocity, water manifested swifter droplet neck evolution. Interestingly, analogous length and velocity parameters were observed for ink and ethanol, suggesting a minimal surface tension influence on droplet ejection velocities. Collectively, it was inferred that fluids with diminished surface tension and augmented viscosity exhibited enhanced droplet morphological preservation until nozzle detachment. Such insights are paramount for comprehending two-phase flow dynamics and their ramifications in varied arenas, spanning from inkjet printing to industrial atomization

procedures.

Figure 5 elucidates velocity distributions along the nozzle axis for the trio of fluids: water, ink, and ethanol. These velocity profiles underpin previous findings, accentuating disparate droplet behaviors across fluids. In water's velocity profile, a pronounced peak proximal to the nozzle aperture was noted, indicative of water droplets undergoing rapid necking and disintegration relative to ink and ethanol. Such characteristics were attributed to water's superior surface tension, facilitating its swifter destabilization and droplet segmentation. Conversely, both ink and ethanol demonstrated congruent velocity profiles along the nozzle trajectory, implying analogous droplet ejection behaviors. Such consistent velocity distributions suggest a more regulated droplet formation trajectory for these fluids. Gleaning insights from these velocity profiles becomes imperative for grasping and optimizing droplet formation across applications, especially in domains like microfluidics and inkjet printing. Recognizing the behavioral nuances of different fluids during ejection equips researchers and engineers to refine parameters to attain specific droplet attributes. This knowledge promises to further technologies reliant on meticulous droplet manipulation, with potential applications in biotechnology, materials science, and digital printing realms.

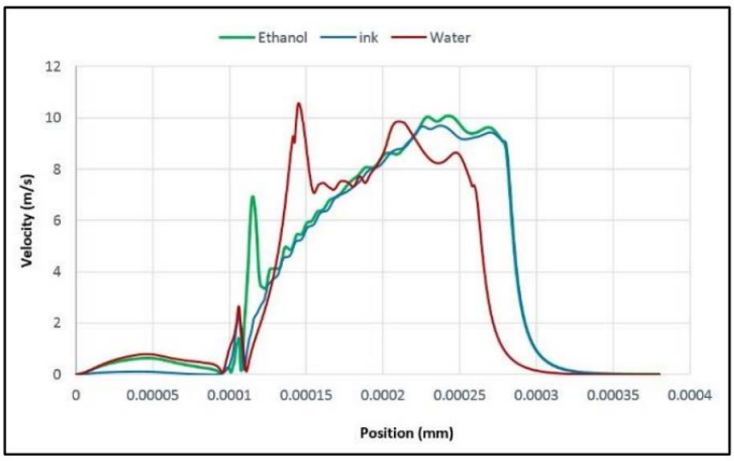


**Figure 5.** Velocity distribution graphs at 18 $\mu$s

## 4 Conclusions

In the conducted study, emphasis was placed on the DOD droplet formation process facilitated by piezoelectric microinjectors, wherein the interplay between fluid properties and excitation levels on the dimensionality of primary and satellite droplets was scrutinized. It was deduced from the results that both surface tension and fluid viscosity play pivotal roles in governing the dynamics of microdroplets.

An augmentation in surface tension, coupled with a decrement in fluid viscosity, was observed to correspondingly increase the size of the primary droplet. Yet, for fluids exhibiting heightened surface tension, such as water, this enlargement in size was observed to potentially instigate the disintegration of the principal droplet into several primary or satellite droplets. Such occurrences were identified as counterproductive in DOD processes, given their propensity to compromise the exactitude of controlled droplet inkjetting.

For the attainment of optimum functionality in microfluidic and inkjet printing endeavors, the selection of a fluid characterized by appropriate surface tension and viscosity was deemed imperative. It was discerned that, by judiciously determining the optimal fluid, the precision of droplet formation could be elevated, thereby ensuring uniformity in droplet dimensions and curtailing the emergence of satellite droplets.

In essence, the elucidation of the influence exerted by fluid properties and excitation levels on droplet genesis was recognized as instrumental for the enhancement of both the efficiency and accuracy intrinsic to inkjet printing and microfluidic modalities. Such cognizance promises to galvanize developments in diverse sectors, encompassing biotechnology, materials science, and digital printing, wherein meticulous droplet formulation is paramount. Prospective investigations could delve into discerning the implications of other fluid attributes, such as compressibility and buoyancy, on droplet formation dynamics.

### Data Availability

Not applicable.

### Conflicts of Interest

The authors declare no conflict of interest.

## References


[1] A. Gao and A. Sonin, "Precise deposition of molten microdrops: The physics of digital microfabrication," in *Proceedings of the Royal Society of London. Series A: Mathematical and Physical Sciences*, 1994, pp. 533–554. https://doi.org/10.1098/rspa.1994.0037

[2] L. Lin and W. He, "Inkjet printing of biosensors for medical diagnostic devices," in *NIP & Digital Fabrication Conference*, 2006, p. 98.

[3] H. Ulmke, T. Wriedt, and K. Bauckhage, "Piezoelectric droplet generator for the calibration of particle-sizing instruments," *Chem. Eng. Technol.*, vol. 24, pp. 265–268, 2001. https://doi.org/10.1002/1521-4125(200103)24:3⟨265::AID-CEAT265⟩3.0.CO;2-4

[4] P. Ben-Tzvi and W. Rone, "Microdroplet generation in gaseous and liquid environments," *Microsyst. Technol.*, vol. 16, pp. 333–356, 2010. https://doi.org/10.1007/s00542-009-0962-7

[5] L. Rayleigh, "On the instability of jets," *Proc. London Math. Soc.*, vol. 1, no. 1, pp. 4–13, 1878. https://doi.org/10.1112/plms/s1-10.1.4

[6] R. Li, N. Ashgriz, and S. Chandra, "Droplet generation from pulsed micro-jets," *Exp. Therm Fluid Sci.*, vol. 32, no. 8, pp. 1679–1686, 2008. https://doi.org/10.1016/j.expthermflusci.2008.06.002

[7] T. W. Shield, D. B. Bogy, and F. E. Talke, "Drop formation by DOD ink-jet nozzles: A comparison of experiment and numerical simulation," *IBM J. Res. Dev.*, vol. 31, no. 1, pp. 96–110, 1987. https://doi.org/10.1147/rd.311.0096

[8] K. C. Chaudhary and T. Maxworthy, "The nonlinear capillary instability of a liquid jet. Part 2. Experiments on jet behaviour before droplet formation," *J. Fluid Mech.*, vol. 96, no. 2, pp. 275–286, 1980. https://doi.org/10.1017/s002211208000211x

[9] A. Amirzadeh Goghari and S. Chandra, "Producing droplets smaller than the nozzle diameter by using a pneumatic drop-on-demand droplet generator," *Exp. Fluids*, vol. 44, pp. 105–114, 2007. https://doi.org/10.1007/s00348-007-0378-z

[10] Y. Wang, J. Bokor, and A. Lee, "Maskless lithography using drop-on-demand inkjet printing method," in *Proceedings SPIE 5374, Emerging Lithographic Technologies VIII*, 2004, pp. 628–636. https://doi.org/10.1117/12.541711

[11] H. Dong, W. W. Carr, and J. F. Morris, "An experimental study of drop-on-demand drop formation," *Phys. Fluids*, vol. 18, no. 7, pp. 72–102, 2006. https://doi.org/10.1063/1.2217929

[12] K. Fan, J. Chen, C. Wang, and W. Pan, "Development of a drop-on-demand droplet generator for one-drop-fill technology," *Sens. Actuators, A*, vol. 147, no. 2, pp. 649–655, 2008. https://doi.org/10.1016/j.sna.2008.03.006

[13] D. B. Wallace, W. R. Cox, and D. J. Hayes, "Direct Write Using Ink-Jet Techniques," in *Direct-Write Technologies for Rapid Prototyping*. Academic Press, New York, 2002, pp. 177–227. https://doi.org/10.1016/b978-012174231-7/50060-9

[14] C. O. Pedersen, "An experimental study of the dynamic behavior and heat transfer characteristics of water droplets impinging upon a heated surface," *Int. J. Heat Mass Transfer*, vol. 13, no. 2, pp. 369–381, 1970. https://doi.org/10.1016/0017-9310(70)90113-4

[15] J. R. Castrejón-Pita, G. D. Martin, S. D. Hoath, and I. M. Hutchings, "A simple large-scale droplet generator for studies of inkjet printing," *Rev. Sci. Instrum.*, vol. 79, no. 7, pp. 75–108, 2008. https://doi.org/10.1063/1.2957744

[16] S. Cheng and S. Chandra, "A pneumatic droplet-on-demand generator," *Exp. Fluids*, vol. 34, no. 6, pp. 755–762, 2003. https://doi.org/10.1007/s00348-003-0629-6

[17] J. C. Carter, R. M. Alvis, S. B. Brown, K. C. Langry, T. S. Wilson, M. T. McBride, M. L. Myrick, W. R. Cox, M. E. Grove, and B. W. Colston, "Fabricating optical fiber imaging sensors using inkjet printing technology: A pH sensor proof-of-concept," *Biosens. Bioelectron.*, vol. 21, no. 7, pp. 1359–1364, 2006. https://doi.org/10.1016/j.bios.2005.06.006

[18] S. Y. Teh, R. Lin, L. H. Hung, and A. P. Lee, "Droplet microfluidics," *Lab Chip*, vol. 8, no. 2, p. 198, 2008. https://doi.org/10.1039/b715524g

[19] M. Seo, C. Paquet, Z. Nie, S. Xu, and E. Kumacheva, "Microfluidic consecutive flow-focusing droplet generators," *Soft Matter*, vol. 3, no. 8, pp. 986–992, 2007. https://doi.org/10.1039/b700687j

[20] J. M. Crowley, "Electrohydrodynamic droplet generators," *J. Electrostat.*, vol. 14, no. 2, pp. 121–134, 1983. https://doi.org/10.1016/0304-3886(83)90001-3